On the preferential concentration of solid particles in turbulent channel flow

By DAMIAN W. I. ROUSON† AND JOHN K. EATON

Mechanical Engineering Department, Stanford University, Stanford, CA 94025, USA

We present results from a direct numerical simulation of the passive transport of solid particles by a fully developed turbulent channel flow with a Reynolds number of 180 based on the friction velocity and the channel half-width. Three particle sets are studied, ranging in diameter from 0.5 to 1.4 viscous wall units and in aerodynamic time constant from 0.6 to 56 centreline Kolmogorov time scales. We use particle number density histograms and fractal dimensions to show that the level of order in the particle spatial distribution peaks near a Stokes number of unity based on the Kolmogorov time scale. We then quantify the relationship between this spatial distribution and the instantaneous flow topology. The results indicate that the previously reported preferential concentration of particles in low-speed streaks leads to a suppression of particle velocities in the viscous sublayer and buffer region even in the presence of streamwise gravitational acceleration. In other regions of the flow, the particles' non-random spatial distribution is shown to be uncorrelated with the local flow topology. We compare our results with the experimental data of Kulick *et al.* (1994) and Fessler *et al.* (1994) and confirm that the latter authors' results were not influenced by turbulence modification.

1. Introduction

1.1. *Motivation and objectives*

Investigating solid particle transport by turbulent fluids provides insight into natural systems, such as urban atmospheres, and technological systems, such as clean room filtration devices. The statistical modelling of particulate transport ranks as one of the classical problems of turbulence research. Yet little is known regarding the detailed dynamics of the phenomenon. By contrast, decades of single-phase flow research is coalescing into a picture of persistent structures arising in a quasi-periodic fashion with random phase shifts. What level of order these structures impart to a dispersed phase remains an open question. In particular, it remains unclear how to relate the particle number density field to the turbulence structure in wall-bounded flows.

This question can be answered in part by direct numerical simulation (DNS) of the turbulence with simultaneous Lagrangian tracking of the particles, which represents the most fundamental approach available. DNS resolves all of the dynamically relevant scales of the turbulence, while the particle equation of motion is built on the well-understood physics of low-Reynolds-number flow around small spheres.

Current computer technology makes this approach feasible for simulating canonical

† Present address: Mechanical Engineering Dept., The City College of The City University of New York, Convent Ave. at 140th St., New York, NY 10031, USA.

flows with particle number densities equal to those of related experiments, albeit at Reynolds numbers below experimental values. Thus, we set out to simulate the flow studied by Kulick, Fessler & Eaton (1994) and Fessler, Kulick & Eaton (1994) at approximately one-fourth their Reynolds number. They were able to measure the level of order in the particle spatial distribution but were unable to relate that order to the turbulence structure. Our work was motivated by the emergence of computational resources sufficient to fill this gap in the empirical database.

1.2. *Related work*

We review here some previous work concerning coherent structures in turbulence and the preferential concentration of particles by those structures. The reader is referred to Rouson, Eaton & Abrahamson (1997) for a broader picture of the particle-laden flow literature.

1.2.1. *Coherent structure*

The recognition of coherent structure in turbulence dates at least to the proposal by Theodorsen (1952, as cited in Robinson 1991) of the hairpin vortex as the primary flow unit sustaining near-wall turbulence. More recently, Robinson (1990) reviewed much of the conventional wisdom on coherent structures in the light of the new accumulation of DNS databases. From these, he synthesized a conceptual model that related the cyclic evolution of the sublayer streaks to buffer-layer quasi-streamwise vortices and outer-region arched vortices. He also noted that the quasi-streamwise vortices typically appear individually rather than in the counter-rotating pairs suggested by the hairpin model.

Despite much attention since Theodorsen's work, no widely accepted definition of coherent structure exists. Most definitions involve subjective choices of cut-off values or reference frames. For example, local pressure minima below some threshold value are frequently used to identify vortex cores. One scheme for rational selection of the employed cut-off values was developed by Chong, Perry & Cantwell (1990). Their scheme involves examining every point from a reference frame translating with the local fluid velocity. Each point is then a critical point of the dynamical system obtained by Taylor expansion of the instantaneous fluid velocity $\boldsymbol{u}$ about a point $\boldsymbol{x}$. For all cases of practical interest, the phase-space trajectory of this dynamical system, and hence the physical-space trajectory of fluid elements, is governed by

$$\frac{\mathrm{d}x_i}{\mathrm{d}t} = u_{i,j} x_j \tag{1.1}$$

where u_i and x_i are the ith Cartesian components of the vectors $\boldsymbol{u}$ and $\boldsymbol{x}$, the subscript comma symbolizes partial differentiation with respect to the subsequent index, and the Einstein summation convention applies.

Chong *et al.* (1990) classified all possible trajectories of the above linear system according to the values of the three invariants of the velocity gradient tensor $u_{i,j}$:

$$P = u_{i,i}, \tag{1.2}$$

$$Q = \tfrac{1}{2}[(u_{i,i})^2 - u_{i,j} u_{j,i}], \tag{1.3}$$

$$R = -\lambda_1 \lambda_2 \lambda_3, \tag{1.4}$$

where λ_1, λ_2, and λ_3 are the eigenvalues of $u_{i,j}$. For incompressible flow ($P = 0$), the discriminant
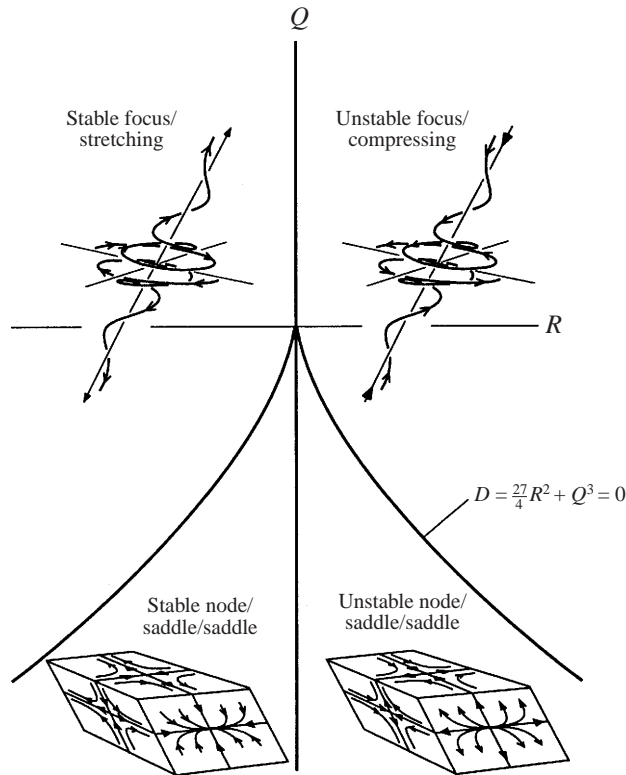
$$D = (27/4)R^2 + Q^3 \tag{1.5}$$

FIGURE 1. Incompressible flow critical point topologies, counterclockwise from upper right: stable focus/compressing, unstable focus/stretching, stable node/saddle/saddle, and unstable node/saddle/saddle (figure courtesy of J. Chacin).

determines the eigenvalues of $u_{i,j}$ and thus the trajectory of x_i. $D > 0$ corresponds to one real and two complex-conjugate eigenvalues; $D < 0$ corresponds to three real, distinct eigenvalues. The curves $D = 0$ and $R = 0$ divide the (Q, R)-plane into the four regions depicted in figure 1: the so-called stable focus/stretching, unstable focus/compressing, stable node/saddle/saddle and unstable node/saddle/saddle critical points.

Blackburn, Mansour & Cantwell (1996) used this scheme to study the topology of fine-scale motions in a turbulent channel flow at $Re_c = 7860$. They discerned high-enstrophy (mean-square vorticity) tubular structures containing aligned vorticity. These structures originate with streamwise orientation in the buffer region, extend obliquely away from the wall through the log layer and attain predominantly spanwise orientation in the wake. They also reported that the viscous dissipation occurs primarily in annular regions surrounding these tubes. However, Jeong & Hussain (1995) later demonstrated that the technique of Chong *et al.* (1990) can mischaracterize the geometry of certain vortical structures due in part to the effect of frame translation. Jeong & Hussain (1995) proposed a vortex definition that is equivalent to that of Chong *et al.* (1990) for planar flows but less error-prone for three-dimensional flows.

1.2.2. *Homogeneous turbulence simulations*

The direct predecessor of the current project was the DNS of particle-laden, homogeneous turbulence by Squires & Eaton (1991). They classified flow structures

according to a four-category scheme developed by Hunt, Wray & Moin (1988) and Wray & Hunt (1989). The four categories were *eddy*, *convergence*, *stream*, and *rotational* zones. Classifying a particular region of the flow involves searching for certain threshold values of the static and dynamic pressure and the second invariant, II, of the velocity gradient tensor:

$$II = u_{i,j}u_{j,i} \equiv S_{ij}S_{ji} - \tfrac{1}{4}\omega_i\omega_i, \tag{1.6}$$

where $S_{ij} = \tfrac{1}{2}(u_{i,j} + u_{j,i})$ is the strain rate tensor and $\omega_k = \epsilon_{ijk}u_{k,j}$ is the vorticity. Eddy zones characterize vortices and therefore correspond to regions of low II and low static pressure p. Convergences zones characterize stagnation points, thus corresponding to high II and high static pressure. Streaming zones characterize fast jets, corresponding to low II and high dynamic pressure. Rotational zones characterize shear layers, corresponding to regions where II is as low as in eddies, but the static pressure is intermediate between that of eddies and convergence zones.

Squires & Eaton (1991) computed the average particle number density found in each of the above zones for particles with Stokes numbers of 0.075, 0.15 and 0.52 based on the integral time scale of a homogeneous turbulent flow. They found the particle number densities to be nearly an order of magnitude higher in convergence zones than in eddies. The number density in rotational zones and streams fell between the other two types of zones, with streams containing more particles per unit volume than rotational zones. They also found that the conditional expectation of particle number densities decreased monotonically with the enstrophy. Finally, they demonstrated the non-randomness of the particle spatial distributions by comparing number density histograms with Poisson distributions of the same mean. In all measures, the peak preferential concentration occurred for the particles with the intermediate Stokes number of 0.15 based on the integral time scale. Wang & Maxey (1993) obtained similar results and argued that peak preferential concentration of particles occurs at a Stokes number of unity when normalized by the Kolmogorov time scale.

J. Segura (private communication) recently investigated the relationship between II and particle location in the centreplane region by post-processing our simulation results. The nearly homogeneous statistics in this region has some similarity to the flows studied by Squires & Eaton (1991) and Wang & Maxey (1993). However, Segura found no noticeable difference between the probability density function of II conditionally sampled at particle locations and those at fluid grid points. (In this region, the streamwise and spanwise grid spacing is uniform and the wall-normal spacing is nearly uniform.) She did discern differences in PDFs calculated for fast-moving particles, which are the particles most likely to have recently visited other regions of the flow.

1.2.3. *Channel flow simulations*

Over the past decade, several research groups have studied some aspect of passive particle transport in channels. Given the narrowness of this topic, it is important to note how the other studies differ from the present work. Since most of the other work has been concerned with deposition and sedimentation, the studies have focused primarily on near-wall behaviour. Small sets of low- to moderate-Stokes-number particles were tracked and assumed to collide inelastically with the channel walls. The present work has concerned primarily Eulerian and Lagrangian statistics, determining the relationship between particle number density and local flow topology, and modelling interphase momentum transfer. None of these tasks would be possible without tracking large ensembles of moderate- to high-Stokes number particles throughout the

entire channel while allowing for resuspension of particles after elastic collision with the wall. Finally, the slip velocities characteristic of such massive particles necessitates the use of a nonlinear drag law, whereas most other DNS studies have simulated Stokesian particles.

McLaughlin (1989) published the first DNS of particle transport in a wall-bounded turbulent flow. He studied aerosol deposition in a fully developed channel flow at the Reynolds number, Re_c, of 2000 based on the mean centreline velocity and channel half-width. The particle Stokes numbers, St^+, were of order one in wall units. The particles accumulated in the viscous sublayer. Depositing particles developed non-negligible slip-velocity Reynolds numbers.

Brooke *et al.* (1992) applied McLaughlin's numerical technique at slightly higher Reynolds number. They found that the slip velocities of depositing particles increased with the particle Stokes number. For the highest Stokes numbers in their study ($St^+ = 10$), the depositing particles' average slip-velocity Reynolds numbers ranged up to 2.5. They used evidence from simulated flow visualization to argue that the eddies responsible for particle deposition are the same quasi-streamwise vortical flow structures responsible for turbulence production. They also noted a weak tendency for particles to accumulate near the wall, where they collect in the low-speed streaks characteristic of the viscous sublayer.

Pedinotti, Mariotti & Banerjee (1992) studied Stokesian particle sedimentation in open channels. They modelled nearly neutrally buoyant particles with a particle equation of motion that balanced inertial effects with Stokes drag and gravity. The particles were assumed to collide inelastically yet frictionlessly with the channel bottom in order to allow for resuspension into the flow. Thus, upon collision, the particles stick and slide. These authors again observed preferential concentration of moderate-Stokes-number particles in low-speed streaks.

They also pointed out that it is impossible to match the particle Stokes number in all relevant scalings for two studies performed at different Reynolds numbers. For example, one can match the Stokes number based on the Kolmogorov time scale, but the Stokes number based on the viscous wall time scale will not match and vice versa. The limitation of DNS to low Reynolds numbers thus makes difficult the comparison with higher-Reynolds-number flows observed in the laboratory. The challenge is to match the scales that are most dynamically relevant to the phenomena under study.

1.2.4. *Channel flow experiments*

We will make direct comparisons between our results and the experimental data of Kulick *et al.* (1994) and Fessler *et al.* (1994). Kulick *et al.* measured Eulerian velocity statistics for the fluid and solid phases in a downward, fully developed channel flow at the Reynolds number $Re_c = 13\,800$. They studied particles ranging in size from $28\,\mu m$ diameter Lycopodium spores to $90\,\mu m$ glass at a range of mass loadings. Their 2% mass-loading case closely approximates our passive particle tracking and will therefore be used for comparison.

Fessler *et al.* studied the particle spatial distribution at the centreplane of the same channel. They used number density histograms and fractal dimensions to quantify the level of non-randomness in the observed distributions. One unresolved question in their study relates to their need to achieve number density histograms with comparable means at varying Stokes numbers. This required varying the mass-loading, which limited their ability to detect preferential concentration of particles in the absence of turbulence modification. For the highest particle Stokes numbers studied, the mass loading was sufficient to attenuate the turbulence intensities as much as 40% in the
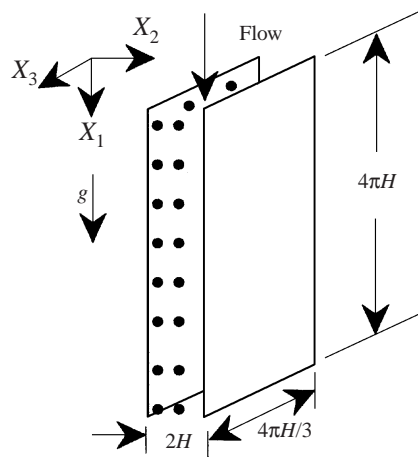
FIGURE 2. Flow configuration.

channel centreplane. DNS with passive particle tracking provides a feasible method for firmly establishing the preferential concentration trends reported by Fessler *et al.*

2. Methodology

For the idealized flow configuration of figure 2, we simulated three particle sets studied by Kulick *et al.* and Fessler *et al.* For these sets, we computed several sets of statistics describing the particle distribution, including number density histograms and fractal dimensions. We also calculated the invariants Q and R both on a uniform grid and on one coincident with the particle locations. Several other flow descriptors, including Eulerian and Lagrangian velocity statistics, are reported in Rouson *et al.* (1997).

The fluid-phase mass and momentum transport were modelled by the three-dimensional, time-dependent, incompressible Navier–Stokes equations supplemented by the incompressibility constraint. The spatial variation of the flow variables was approximated by the spectral representation of Kim, Moin & Moser (1987), which implies no-slip boundary conditions at the solid walls and periodic boundary conditions at the streamwise- and spanwise-normal boundaries. We employed their spatial resolution of 128 Fourier modes in the statistically homogeneous streamwise (X_1) and spanwise (X_3) directions and 129 Chebyshev modes in the wall-normal (X_2) direction with an expansion by $3/2$ in X_1 and X_3 for de-aliasing purposes when calculating the nonlinear terms. We coupled this spatial representation with the third-order Runge–Kutta (RK3) time-advancement algorithm developed by Spalart, Rogers & Moser (1991). The initial velocity field was the output from a single-phase flow DNS in which randomly perturbed, plane Poiseuille flow was advanced in time until its Eulerian statistics reached a stationary state.

Since the drag expression of Stokes (1851) underpredicts the drag at the particle slip-velocity Reynolds numbers observed by previous investigators, we applied a correction factor that matches experimental drag measurements to within 5% up to slip-velocity Reynolds numbers of 800 (Schiller & Nauman 1933, as cited in Clift, Grace & Weber 1990). With this correction, our final equations of motion for a

		Simulation	Experiment
Fluid			
	$Re_{\bar{q}}$	3297	13 800
	Re_{τ}	180	640
28 µm diameter Lycopodium			
	St_K	0.60	0.60
	St^+	8.6	22
	a/H	0.00070	0.00070
50 µm diameter Glass			
	St_K	8.1	8.1
	St^+	117	300
	a/H	0.00125	0.00125
70 µm diameter Copper			
	St_K	56	56
	St^+	810	2000
	a/H	0.00175	0.00175

TABLE 1. Flow and particle parameters. ($Re_{\bar{q}}$ and Re_{τ} are the Reynolds numbers based on the mean centreplane velocity and the friction velocity, respectively. St_K is the Stokes number based on the Kolmogorov time scale.)

particle at position $\boldsymbol{r}$ with velocity $\boldsymbol{v}$ at time t are

$$\frac{\mathrm{d}r_i}{\mathrm{d}t} = v_i, \tag{2.1}$$

$$\frac{\mathrm{d}v_i}{\mathrm{d}t} = \frac{C_D Re_p}{24 St} \left[u_i(\boldsymbol{r}, t) - v_i(t) \right] + g_i, \tag{2.2}$$

$$C_D \equiv \frac{24}{Re_p} (1 + 0.15 Re_p^{0.687}), \tag{2.3}$$

where C_D and Re_p are the drag coefficient and Reynolds number based on slip velocity and particle diameter. The fluid velocity was obtained in (2.2) by three-dimensional linear interpolation between the spectral collocation points. Equations (2.1)–(2.3) were time-advanced with the same RK3 scheme as used for the fluid phase.

Table 1 provides the channel flow Reynolds numbers, the particle Stokes numbers and the particle radii, a, normalized by the channel half-width, H, for the present simulations and for the experiments. Note that we matched the Stokes numbers based on the Kolmogorov time scale. Fessler *et al.* and Wang & Maxey (1993) found that this parameter determines the level of preferential concentration in the particle spatial distribution.

Although not employed in the results presented here, we investigated the inclusion of the lift force due to Saffman (1965). McLaughlin (1989) found that this lift force increased the deposition velocity of simulated aerosol particles. Similarly, our tests showed that lift increased the rate of particle accumulation near the wall; however, it did not influence the Eulerian velocity statistics. This might be expected since the term is formally of the same order in particle radius as several terms we neglected in the more complete equation of motion derived by Maxey & Riley (1983). Finally, we also tested a lift expression that McLaughlin (1993) derived with less restrictive assumptions, but that term proved negligible compared to the particle drag in the same direction.

We tracked 72^3 particles for each of the three particle sets listed in table 1, providing number densities comparable to those used for the preferential concentration studies of Fessler *et al.* The particles were initially seeded uniformly on a three-dimensional rectangular grid. The dispersed-phase boundary conditions were periodicity in the streamwise and spanwise directions and specular reflection at the wall. Periodicity implies that particles exiting the flow domain through one boundary were reintroduced at the opposing boundary with their exiting velocity.

Simulations were run until the particles' Eulerian velocity statistics became stationary in time. The number density statistics, however, never achieve stationarity owing to a steady accumulation of all particle sets in the channel core and an accumulation of the two smaller types of particles near the wall. The core accumulation stems from turbulence intensities being too low there to support significant dispersion. The near-wall accumulation (which has also been observed by McLaughlin 1989, Brooke *et al.* 1992 and Pedinotti *et al.* 1992) we attribute to the low Reynolds number and the particle size. The smaller particles do not extend far enough from the wall to interact with the flow structures responsible for sweeping the larger particles away. One could also argue that the larger particles possess more momentum and therefore rebound further upon striking the wall. However, even these particles were trapped near the wall in a DNS we performed at a lower Reynolds number (Rouson & Eaton 1994).

Despite this trapping phenomenon, the particle velocity statistics become stationary after a few fluid time scales or particle time constants, whichever is larger. Eulerian velocity statistics were averaged over X_1, X_3, t, and over the direction of reflectional symmetry on either side of the channel centreplane. All of this was implemented in the Vectoral language on a Cray C-90 at the Pittsburgh Supercomputer Center. The reader is referred to Rouson *et al.* (1997) for discussion of the software implementation and the attendant issues of numerical stability and accuracy.

3. Results

3.1. *Particle distribution*

Two extremes exist in dispersed particles' response to turbulence. High-Stokes-number particles respond to so little of the spectrum of turbulent eddies that their motion lacks coherent mechanisms for non-random clustering. Low-Stokes-number particles act as flow tracers. Their mean spacing is fixed by the continuity constraint, so they are precluded from clustering near a point.

Between these two extremes exists a range of Stokes numbers within which particles respond to some eddies but not to others. One expects these particles to preferentially concentrate in certain flow structures. Examples are the clustering of particles in convergence zones (cf. Eaton & Fessler 1994) and the aforementioned clustering of particles in low-speed streaks of wall-bounded flows.

Precisely which structures cause preferential concentration varies from flow to flow. Whereas the large vortex rings characteristic of forced jets might be responsible for the preferential concentration in that flow (cf. Longmire & Eaton 1992), the small, dissipative eddies that result from strong vortex stretching might be responsible in other flows (cf. Wang & Maxey 1993). In the former case, the Stokes number based on the large-eddy turnover time would determine the level of non-randomness in the particle distribution, whereas in the latter case, the Stokes number based on the Kolmogorov time scale might be more relevant. Whichever is the case, none of

the state-of-the-art models for turbulent dispersion are capable of predicting such structural behaviour. We seek here to parametrize this behaviour for channel flow.

Figure 3 gives direct visual evidence that the smallest of our particles are distributed in a non-random fashion at the channel centreplane. The Lycopodia show large voids surrounded by bands of high concentration. Similar behaviour was discerned in the Lycopodium particles illuminated by a laser sheet at the centreplane of the Fessler *et al.* wind tunnel. The simulated glass particles exhibit voids but primarily along lengthy streamwise bands reminiscent of the near-wall streaks. In the experimental photographs of Fessler *et al.*, one might argue there exists some structure on the scale of the photograph's dimensions, but there is not the streakiness of the simulation. The copper distributions appear random for both the DNS and the experiment. Neither significant voids nor distinct clusters appear in either case.

The presence of streaks in the simulated glass distributions deserves further discussion since it was not observed in the experiment. The most likely reason for the difference is the Reynolds number difference. In the simulations, the near-wall region containing the longitudinal vortices occupies a larger fraction of the channel. Particles collected in the low-speed streaks are swept outward all the way to the channel centreplane by these near-wall vortices. Also, note that the Stokes number based on wall variables is smaller in the simulation since we match the Stokes numbers based on the Kolmogorov scale. The collection of particles in the low-speed streaks is probably best characterized by St^+. It will be shown in §3.2 that there is no correlation between particle location and local turbulence structure in the centreplane region. Therefore, the concentration distribution at the centreplane must be an artifact of structure closer to the wall.

Fessler *et al.* digitized multiple photographs and plotted histograms of the particle number density computed on a regular grid of square cells. They compared the resulting curves with the expected histograms for randomly distributed particles. Here 'random' is defined as the situation in which any given particle is equally likely to appear in any given cell. With only this condition, one can show that the number of particles per cell is binomially distributed and that this binomal distribution approaches a Poisson distribution as the total numbers of particles and cells increases while holding their ratio constant. For the number of particles and cells employed here, the terms 'binomial' and 'Poisson' are interchangeable.

The Poisson distribution is characterized by a single parameter, the mean value. Hence, Fessler *et al.* compared the actual particle histograms with Poisson distributions of the same mean. Such comparisons obviously depend on the cell width chosen. At cell widths smaller than the Kolmogorov length scale, there exist no turbulent eddies to generate preferential concentration. At cell widths greater than the channel width, the histograms are averaged over multiple large eddies. It follows that histograms computed on very fine grids and very coarse grids will be randomly distributed, whereas distributions computed with intermediate cells can be non-random.

We assembled histograms from eleven snapshots of the particles near our channel centreplane, each snapshot separated by approximately 40 wall units in time. Each snapshot contained approximately 2000–3000 particles, so $N_p \approx 22\,000$–$33\,000$. We divided each image into at least 75 cells and at most 4800, so $N_c = 825$–$52\,800$.

Figure 4 shows the calculated particle histograms at the cell width of peak deviation from randomness for each particle set. We will not make a direct comparison of these to the experiments since that would require matching the mean number of particles per cell. The figure does, however, show binomial distributions with the same N_p and N_c for comparison. Note that the cell width for maximum particle organization, $\varDelta$,
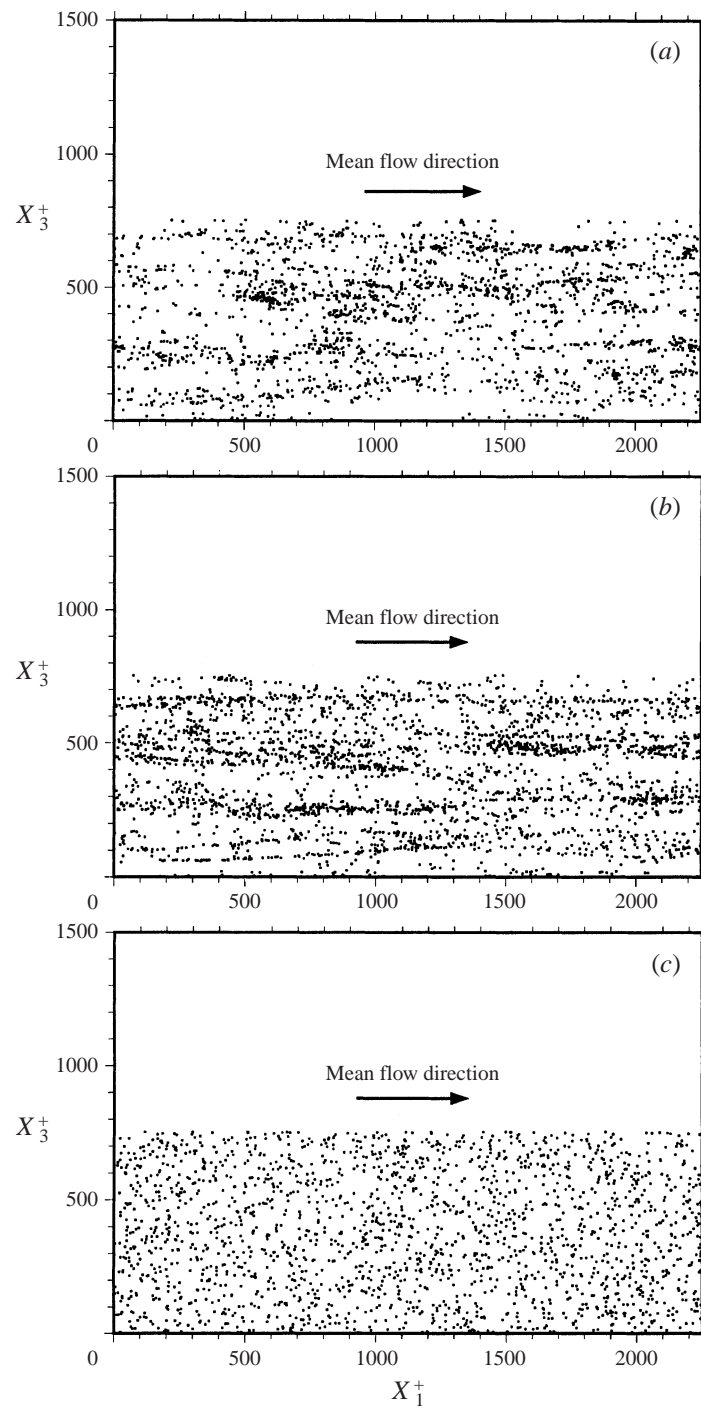
FIGURE 3. Particles near channel centreplane: Lycopodia (*a*), glass (*b*), copper (*c*). Each plot shows particles across the entire channel width (approximately 754 wall units), above which white space is added for labelling purposes.
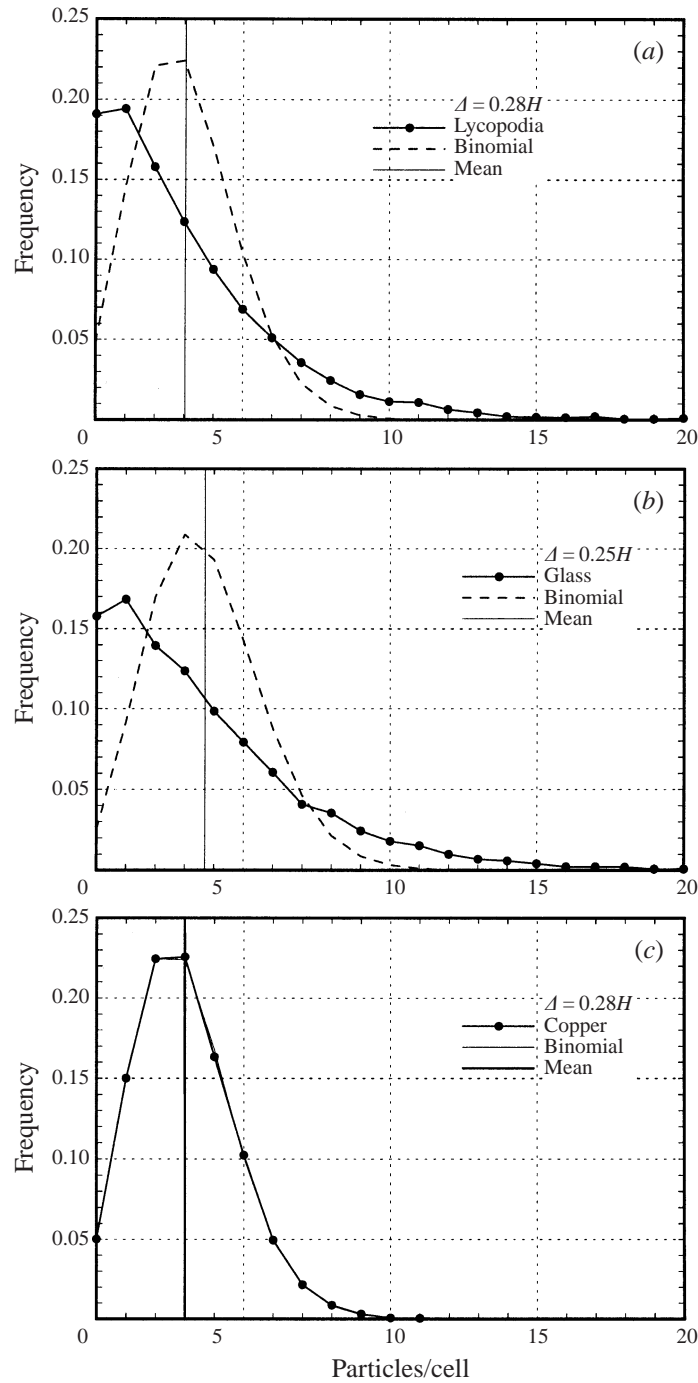
FIGURE 4. Particle number density histograms at maximum coherence:
Lycopodia (*a*), glass (*b*), copper (*c*).

ranges from 0.25*h*–0.28*h*, which is approximately 125 times the Kolmogorov length
scale at the channel centreplane. It can be clearly discerned from the figure that the
copper particles are randomly distributed at this scale. This was true at all length
scales studied. The Lycopodia and the glass particles, however, exhibit considerable
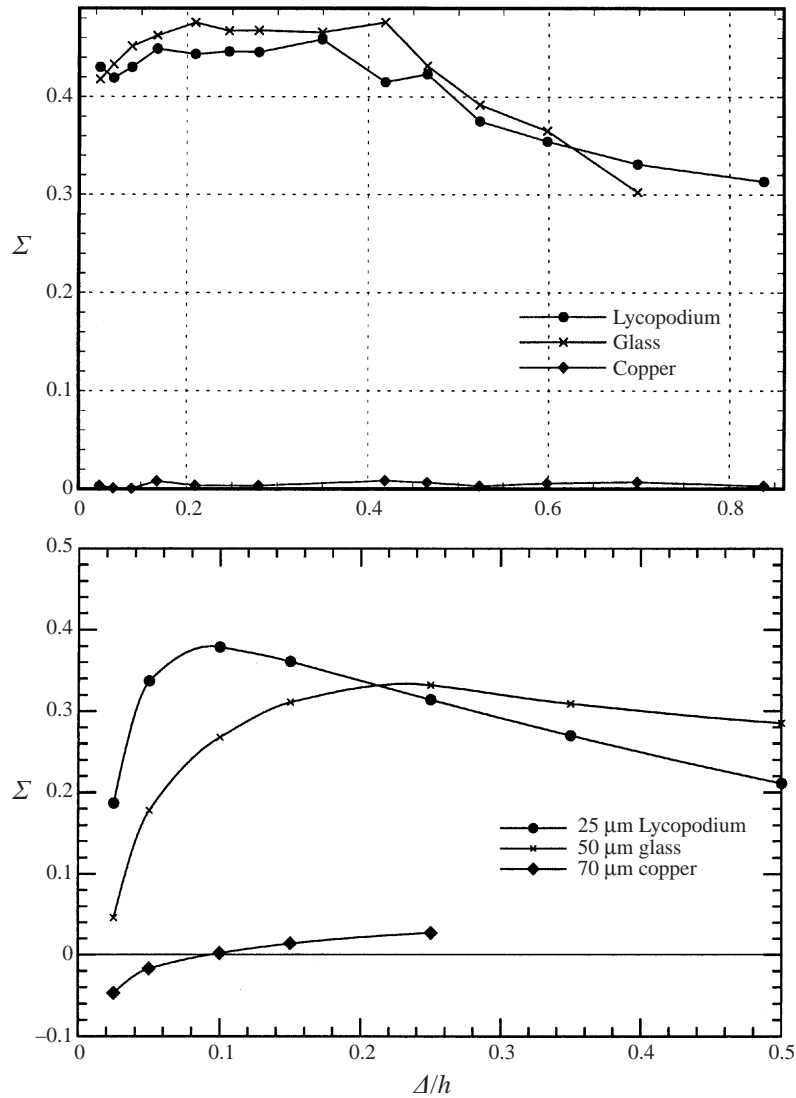
FIGURE 5. Variation of distribution randomness with cell width normalized by channel half-width: simulation (*a*) and experiment (*b*).

deviation from randomness at the scale shown. They are more randomly distributed at both larger and smaller scales, not shown here.

To illustrate this trend, we use a parameter that describes each distribution's deviation from randomness:

$$\Sigma \equiv \frac{\sigma - \sigma_{\text{Poisson}}}{\lambda}, \qquad (3.1)$$

where σ and σ_{Poisson} are the standard deviations of the actual and Poisson distributions, respectively, and λ is the mean value. For particles preferentially concentrated by turbulence, one expects large positive values of Σ corresponding to a flat distribution. Randomly distributed particles generate values of Σ near zero.

Figure 5 shows the variation of Σ with cell width for the simulation as well as for the experiment. In both cases, we see the aforementioned trends, that is
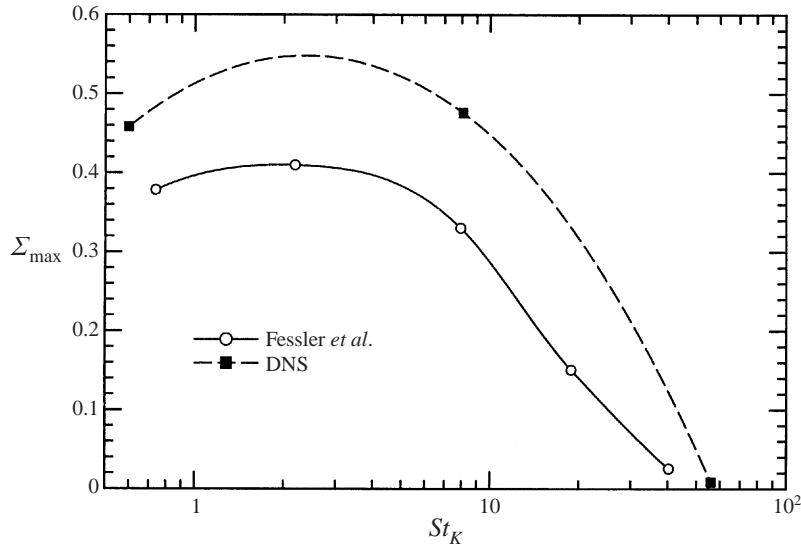
FIGURE 6. Dependence of maximal non-randomness on Stokes number (based on the Kolmogorov time scale).

maximum randomness (minimum Σ) at very small and very large length scales with minimum randomness (maximum Σ) occurring at intermediate cell size widths. Both the DNS and experiment show that the copper particles' distribution deviates little from randomness at any length scale and that the non-randomness of the Lycopodia and the glass are of the same order. The Σ values for these two particle sets should vanish at much greater and smaller scales, but studying smaller scales would require more particles, and larger scales more snapshots, than the current flow domain and computational resources allow.

Figure 6 shows the peak deviation from randomness, Σ_{max}, for the three particle sets studied. It is difficult to determine detailed trends given only three data points; however, the simulation data are consistent with the observation of Fessler *et al.* that the point of peak Σ_{max} is of $O(1)$.

Fessler *et al.* pointed out that the results shown in figure 6 left some ambiguity as to which particles are most affected by the turbulence. Those in figure 5 implied that the answer to this question depended on the length scale at which one asks the question. Thus, they employed the correlation dimension introduced by Grassberger & Procaccia (1983) and first applied to particulate distributions by Tang *et al.* (1992). The correlation dimension is computed by choosing a base particle in one of the centreplane snapshots and then counting the number, N, of particles within a circle of radius ℓ centred at the base particle. For this purpose, we projected all particles in the snapshot onto the centreplane. If the particles uniformly cover this two-dimensional space, then N will scale with the area of the circle ($N \propto \ell^2$). If the particles are organized along thin lines, N will scale linearly with ℓ. Between these extremes, N scales with some fractional power of ℓ. This power is the correlation dimension, v, a fractal descriptor of the particle spatial distribution. One expects $v \rightarrow 2$ as $St_K \rightarrow 0$ and as $St \rightarrow \infty$.

We chose ten values of ℓ in the range 0.2–0.4 channel half-widths, the range over which preferential concentration is strongest in figure 5. For each value of ℓ, we averaged N over 1000 base particles in each of the eleven snapshots used for figure
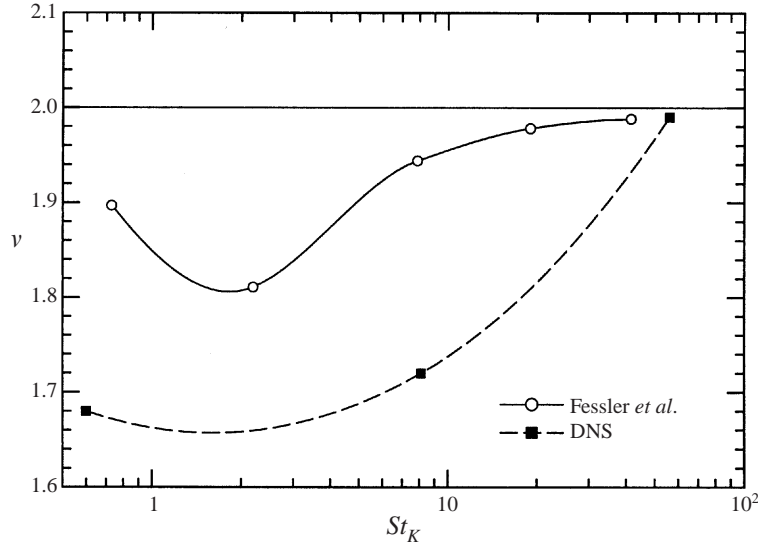
FIGURE 7. Dependence of correlation dimension on Stokes number (based on the Kolmogorov time scale).

5. Figure 7 shows the resulting values of v for each Stokes number studied in the experiment and the DNS. Again the Lycopodia and glass particles exhibit similar levels of preferential concentration whereas the copper particles are more randomly dispersed than both. Again the DNS results are consistent with the experimental result of peak non-randomness at $St_K \sim 1$.

3.2. *Flow topology*

We next seek to relate this non-randomness to coherent flow structures using the structural classifcation scheme employed by Blackburn *et al.* (1996). This scheme was chosen over that of Hunt *et al.* (1988) because the Blackburn *et al.* scheme provides an objective classification that eliminates the arbitrary choice of threshold values used in the Hunt *et al.* algorithm. Single parameter descriptors, such as vorticity magnitude or II, cannot uniquely select a structure type. Blackburn *et al.* (1996) showed that all topologies in incompressible flow fall into the four types illustrated in figure 1: unstable focus/compressing, stable focus/stretching, stable node/saddle/saddle and unstable node/saddle/saddle. The first two are vortical flow regions. The last two are essentially convergence zones. We applied this classification system to the same eleven fields studied in §3.1. Thus, we computed Q and R at each fluid grid point in each of four regions: the viscous sublayer ($y^+ < 5$), the buffer region ($5 \leqslant y^+ < 35$), the logarithmic layer ($35 \leqslant y^+ < 150$), and the core region ($y^+ \geqslant 150$). We also conditionally sampled Q and R at the positions of solid particles in order to determine if the particles show any preference for or against any of the aforementioned four topologies.

Figure 8 shows four decades of the resulting joint probability density function (PDF) of Q and R in the viscous sublayer. Note that Q and R are both zero for the mean flow, and that zero is their most probable value for all instantaneous realizations studied. Moving away from the origin, the PDF sampled at the fluid grid points shows the same preference for the second and fourth quadrants that Blackburn *et al.* found in other regions of the flow. They, however, studied only one instantaneous realization
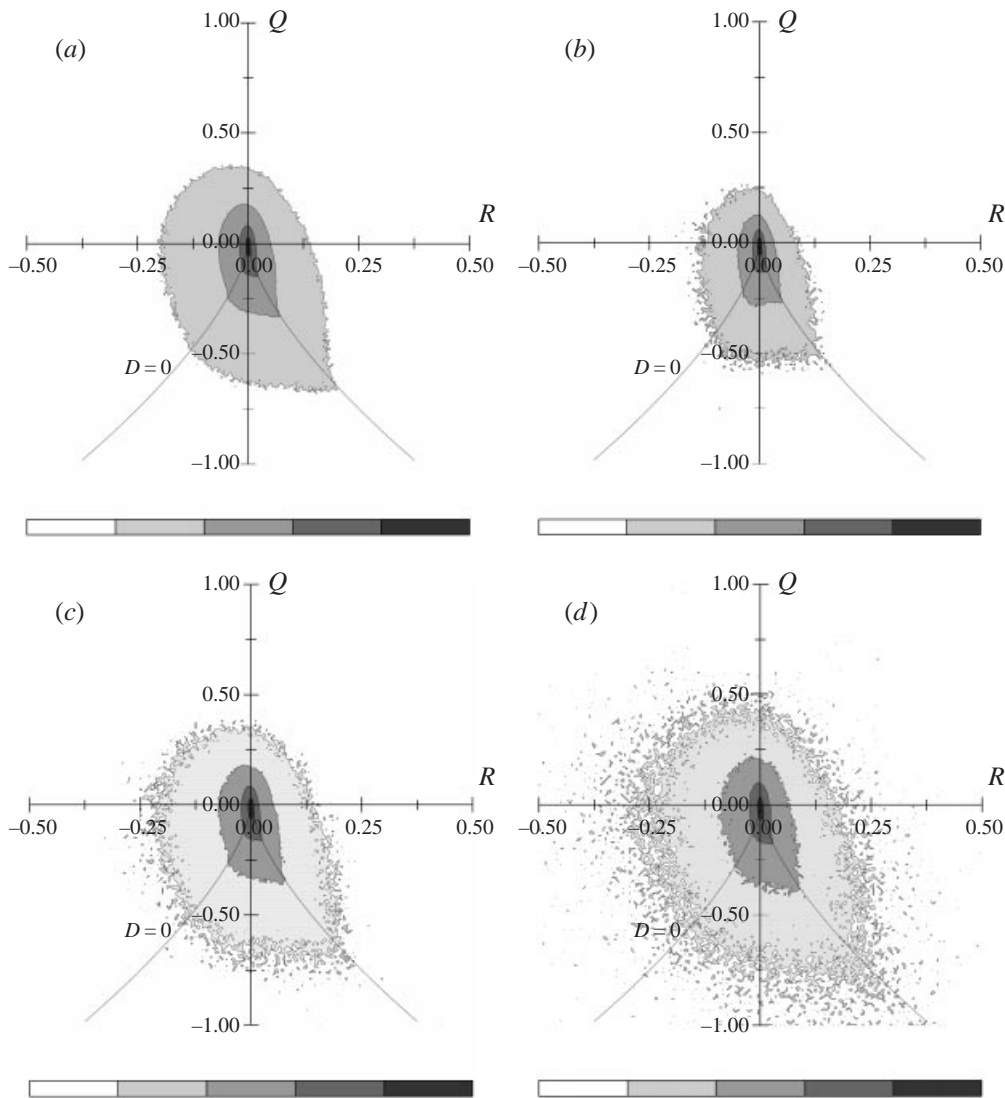
FIGURE 8. Viscous sublayer ($X_2^+ < 5$) joint PDF of Q, R conditionally sampled at fluid grid points (*a*), Lycopodium particle positions (*b*), glass particle positions (*c*), and copper particle positions (*d*).

and thus did not have enough samples to document this trend in the viscous sublayer. The preferred quadrants correspond to the stable focus/stretching and the unstable node/saddle/saddle topologies. The points associated with the latter topologies are found along the positive-R side of the $D = 0$ line, indicating that the most of the high-strain-rate eddies are near-vortical in some sense, providing evidence of the predominance of vortex stretching in turbulence.

Conditionally sampling this PDF at the positions of the Lycopodium spores produces strikingly different results. The Lycopodia clearly do not sample the strongest vortical regions in either of the first two quadrants. The streamline curvature characteristic of foci flings particles out of the vortex core. This mechanism is enhanced in the second quadrant by outflow from the critical point along the vortex axis of symmetry (cf. figure 1). The particles also avoid the strongest vortex-stretching regions
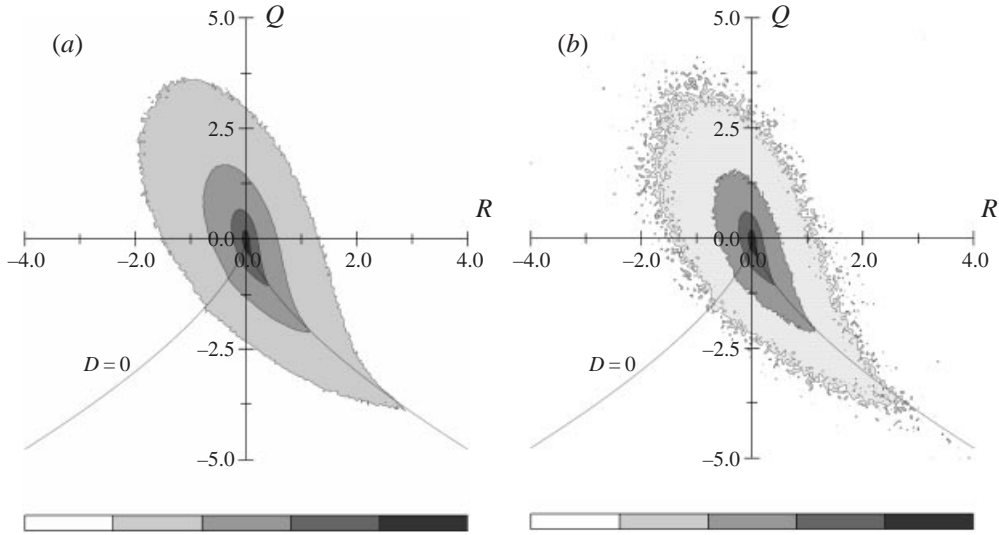
FIGURE 9. Buffer region ($5 \leqslant X_2^+ < 35$) joint PDF of Q, R conditionally sampled at fluid grid points (*a*) and Lycopodium particle positions (*b*).

along the positive-R, zero-D line. The one region of Q, R space not much affected by the conditional sampling is the stable node/saddle/saddle region in the third quadrant. Topologies in this region have two principle axes along which the flow converges toward the critical point, thus providing a mechanism for accumulating particles. The effectiveness of this mechanism is limited, however, by the incompressibility constraint, which requires outflow on the third axis. The unstable focus/stretching topology of figure 1 is the only one for which no such limiting factor exists. Both the flow along the symmetry axis and the surrounding vortex can be expected to induce low particle number densities.

The above results corroborate the visual evidence presented elsewhere by the current authors (Rouson & Eaton 1994) showing that the particle distribution in the viscous sublayer is very closely related to the coherent structure in that region. This statement is less true for the glass particles and completely false for the copper particles. The PDFs of figure 8 correspondingly show the glass position samples approaching the fluid curves. Sampling at copper positions appears to produce an even broader PDF than the fluid; however, this PDF is poorly resolved because of the difficulty in obtaining a large number of samples in the sublayer for particles too big to fit very close to the wall and large enough to be easily swept away from it.

We have observed similar behaviour in the other three flow regions, but the trends become progressively less pronounced with increasing distance from the wall. Figures 9–11 show the same plots for the fluid grid points and conditionally sampled at the Lycopodium positions in the buffer, logarithmic, and core regions of the flow. It is apparent that the particles are much more randomly dispersed relative to the turbulence structures than in the sublayer. Similar trends were observed for the other two sets of particles studied. Far from the wall, conditionally sampling Q and R at particle positions yields plots equivalent to sampling on a uniform grid. This fact deserves further discussion in the light of the clear evidence presented in §3.1 that the smaller particles are distributed non-randomly at the channel centreplane. Two causes appear likely: either the structures responsible for that non-random
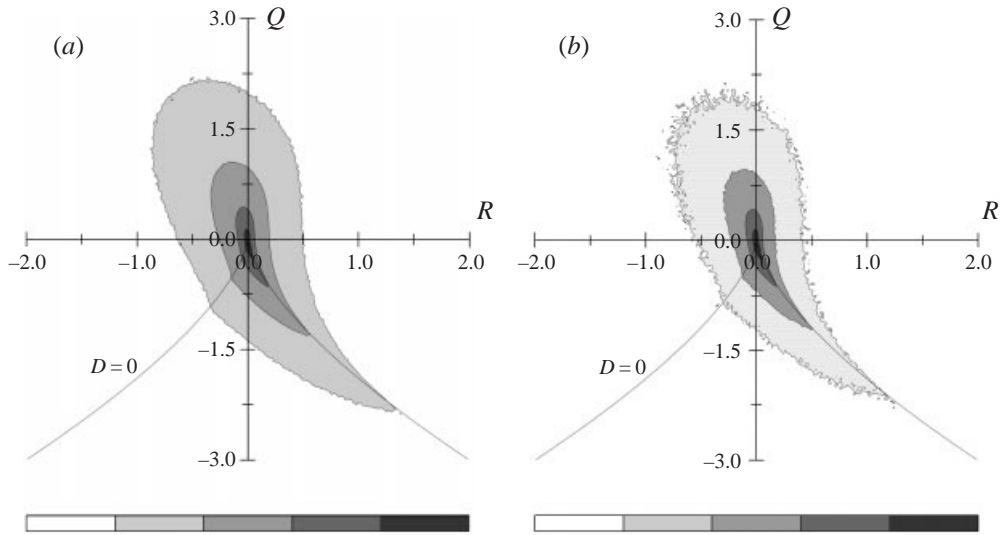
FIGURE 10. Logarithmic-layer ($35 \leqslant X_2^+ < 150$) joint PDF of Q, R conditionally sampled at fluid grid points (*a*) and Lycopodium particle positions (*b*).
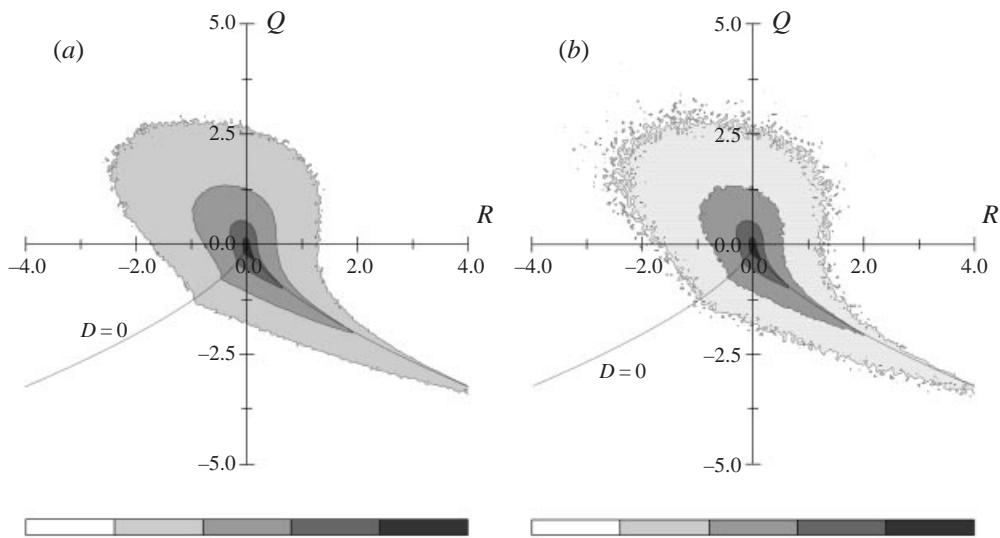

FIGURE 11. Core-region ($X_2^+ \geqslant 150$) joint PDF of Q, R conditionally sampled at fluid grid points (*a*) and Lycopodium particle positions (*b*).

distribution are not collocated with the particle clusters they induce or they are too weak in this measure to detect anything meaningful. Recall the centreplane streaks in the glass particle snapshot of figure 3. Such streaks are more characteristic of near-wall turbulence. Combine this with the fact that the vortical structures in the outer flow have predominantly spanwise orientation (Robinson 1990) and that the invariants decrease dramatically away from the wall. Blackburn *et al.* (1996) showed Q decreasing by two orders of magnitude from the buffer region to the core region at a mean-flow Reynolds number twice ours. Since Q only scales linearly with mean-flow Reynolds number, the decrease would be of the same order in our case. Finally, note
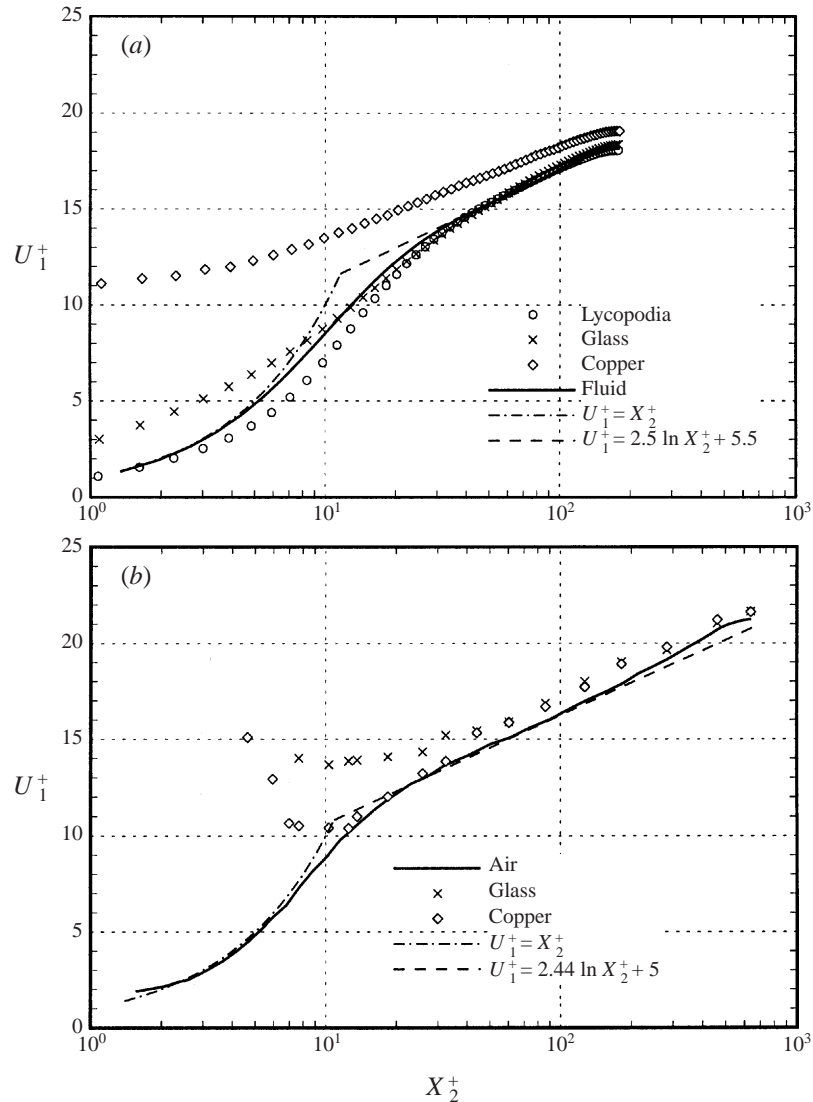
FIGURE 12. Mean streamwise velocity components: Simulation (*a*) and experiment (*b*).

that the non-collocation hypothesis would most affect those particles light enough to preferentially concentrate but massive enough to attain significant slip velocities. The glass particles best fit this description. Thus, it seems likely that a combination of weaker turbulence at the centreplane and particle slip complicates the task of relating centreplane particle distributions to flow structure.

3.3. *Eulerian statistics*

From the non-random distribution of the particles in both physical and phase space, one might expect the particle velocity and number density statistics to differ appreciably from those for fluid elements. We now substantiate this hypothesis by examining mean velocities and number density profiles.

Figure 12 presents the fluid- and solid-phase mean velocities from the present

simulation and the experiment of Kulick *et al.*, all normalized by conventional wall variables. The figure clearly demonstrates that the preferential concentration of the lighter particles in low-speed streaks acts against the streamwise gravitational acceleration and supresses the particles' mean velocities to below that of the fluid. Consequently, the Lycopodia lag the flow throughout the buffer region and well into the viscous sublayer. The glass particles do so only in the upper part of the buffer region. Note that this region contains the strong vortices responsible for turbulence production. These vortices likely have a centrifuge-like effect that separates out the moderate-Stokes-number particles. The ones that deposit in the near-wall region are then induced towards the low-speed streaks by the vortices (cf. Robinson 1990) causing the preferential concentration noted by previous authors. The most important conclusion to be drawn from the present results is that even first-order velocity statistics would be difficult to predict with a statistical model devoid of structure information. Such models have only recently been proposed for single-phase flow (cf. Kassinos & Reynolds 1999). The authors know of none for particle-laden flow.

The copper particles have the most inertia. Therefore, they lead the flow throughout the channel. Although their absolute velocities decrease on approaching the wall, their slip velocities increase dramatically there. The experiment shows qualitatively similar behaviour except near the wall, where the absolute particle velocities increase near the wall. This sort of behaviour is observed early in the simulation as fast-moving particles from the core region mix into the initially vacant near-wall region. Over time, the near-wall velocities decrease to the values shown. This trend indicates that a combination of non-uniform loading and insufficient wind tunnel development length could produce the excessive near-wall velocities in the experiment. The experiment includes a 5.2 m long development section which takes the copper particles 5 to 8 time constants to traverse. However, the development section of the channel was fashioned from particle board whereas the test section was acrylic. A. D. Paris (private communication) recently examined the possible effects of roughness in the development section following the analysis of Sommmerfeld (1992). Sommerfeld argued that the particles' motion is wall-collision dominated when their radii satisfy

$$a \geqslant \frac{1}{2}\sqrt{\frac{18\mu h}{0.7 v_p' \rho_p}} = 60\,\mu\text{m}, \tag{3.2}$$

where ρ_p is the particle mass density and where the final value was computed by Paris for the laboratory conditions of Kulick *et al.* The motion of the 70 μm diameter copper particles must be considered collision-dominated by the above measure. Hence, the accuracy of the particle–wall interaction model is critical to simulating the Kulick *et al.* experiment. Our choice of specular reflection corresponds to assuming frictionless, elastic collisions with a smooth wall. While this model approximates well the acrylic test section where Kulick *et al.* made their measurements, it probably does not match well their particle-board development section upstream of the measurement stations.

4. Conclusions

Direct numerical simulations of low-Reynolds-number turbulent channel flow were performed with Lagrangian tracking of a large number of passive particles. The particle parameters were chosen to match those for three sets of particles studied experimentally by Kulick *et al.* (1994). The channel flow Reynolds number of the experiments was too large to match in the simulations. However, overall trends in the

particle spatial distribution were captured by the simulations, justifying the use of the simulations to evaluate statistics unavailable experimentally.

Particles with Stokes numbers based on the Kolmogorov time scale of the order of unity were preferentially concentrated into longitudinal bands extending across the entire channel, whereas the larger particles remained randomly distributed. This dependence of the spatial distribution on the Stokes number supports earlier findings of Squires & Eaton (1991) and Wang & Maxey (1993) in homogeneous turbulence simulations. It also corroborates the experimental observations of Fessler *et al.* (1994) in the fully developed channel flow and resolves the issue of whether their results were affected by modification of the turbulence.

The topological descriptors developed by Blackburn *et al.* (1996) were used to determine the correlation of the particle positions with the local flow topology. Very near the wall, strongly vortical regions described as focii in the topological classification are depleted of particles as would be expected if the local flow is producing the concentration inhomogeneity. The resultant accumulation of particles in low-speed streaks supresses their mean velocity below the fluid mean velocity at the same wall-normal location. Farther away from the wall, similar levels of concentration non-uniformity were observed. However, the concentration fluctuations away from the wall were not correlated with the topological descriptors. This indicates that the concentration inhomogeneities are formed in the intense turbulence near the wall and then are convected into regions of less intense turbulence where they break down slowly.

REFERENCES

BLACKBURN, H. M., MANSOUR, N. N. & CANTWELL, B. J. 1996 Topology of fine-scale motions in turbulent channel flow. *J. Fluid Mech.* **310**, 269–292.

BOYCE, W. E. & DiPRIMA, R. C. 1977 *Elementary Differential Equations.* John Wiley & Sons.

BROOKE, J. W., KONTOMARIS, K., HANRATTY, T. J. & McLAUGHLIN, J. B. 1992 Turbulent deposition and trapping of aerosols at a wall. *Phys. Fluids* A **4**, 825–834.

CHONG, M. S., PERRY, A. E. & CANTWELL, B. J. 1990 A general classification of three-dimensional flow fields. *Phys. Fluids* A **2**, 765–777.

CLIFT, R., GRACE, J. R. & WEBER, M. E. 1990 *Bubbles, Drops and Particles.* Academic.

EATON, J. K. & FESSLER, J. R. 1994 Preferential concentration of particles by turbulence *Intl J. Multiphase Flow* **20**, 169–209 (supp. issue).

FESSLER, J. R., KULICK, J. D. & EATON, J. K. 1994 Preferential concentration of particles in a turbulent channel flow. *Phys. Fluids* **6**, 3742–3749.

GRASSBERGER, P. & PROCACCIA, I. 1983 Measuring the strangeness of strange attractors. *Physica* D **9**, 189.

HUNT, J. C. R., WRAY, A. A. & MOIN, P. 1988 *Proc. Center for Turbulence Research Summer Prog., Stanford, California*, pp. 193–208.

JEONG, J. & HUSSAIN, F. 1995 On the identification of a vortex. *J. Fluid Mech.* **285**, 69–94.

KASSINOS, S. C. & REYNOLDS, W. C. 1999 Developments in structure-based turbulence modeling. In *Modeling Complex Turbulent Flows* (ed. M. D. Salas, J. N. Hefner & L. Sakell), pp. 69–88. Kluwer.

KIM, J., MOIN, P. & MOSER, R. D. 1987 Turbulence statistics in fully developed channel flow at low Reynolds number. *J. Fluid Mech.* **177**, 133–166.

KULICK, J. D., FESSLER J. R. & EATON, J. K. 1994 Particle response and turbulence modification in fully-developed channel flow. *J. Fluid Mech.* **277**, 109–134.

LONGMIRE, E. K. & EATON, J. K. 1992 Structure of a particle-laden round jet. *J. Fluid Mech.* **236**, 217–257.

McLAUGHLIN, J. B. 1989 Aerosol deposition in numerically simulated channel flow. *Phys. Fluids* A **1**, 1211–1224.

McLAUGHLIN, J. B. 1993 The lift on a small sphere in wall-bounded linear shear flows. *J. Fluid Mech.* **246**, 249–265.

MAXEY, M. R. & RILEY, J. J. 1983 Equation of motion for a small rigid sphere in nonuniform flow. *Phys. Fluids* **26**, 883–889.

PEDINOTTI, S., MARIOTTI, G. & BANERJEE, S. 1992 Direct numerical simulation of particle behaviour in the wall region of turbulent flow in horizontal channels. *Intl J. Multiphase Flow* **18**, 927–941.

ROBINSON, S. K. 1990 A perspective on coherent structures and conceptual models for turbulent boundary layer physics. *AIAA Paper* 90-1638.

ROUSON, D. W. I. & EATON 1994 Direct numerical simulation of turbulent channel flow with immersed particles. In *Numerical Methods in Multiphase Flows*. ASME FED, vol. 185, 47–57.

ROUSON, D. W. I., EATON, J. K. & ABRAHAMSON, S. C. 1997 A direct numerical simulation of a particle-laden turbulent channel flow. *Rep.* TSD-101. Mechanical Engineering Dept., Stanford University.

SAFFMAN, P. G. 1994 The lift on a small sphere in a slow shear flow. *J. Fluid Mech.* **22**, 385–400 and corrigendum **31**, 624.

SCHILLER, L. & NAUMAN, A. Z. 1933 *Ver. Deut. Ing* **77**, 318–320 (cited in Clift, Grace, & Weber 1978).

SOMMERFELD, M. 1992 Modelling of particle-wall collisions in confined gas-particle flows. *Intl J. Multiphase. Flow* **18**, 905–926.

SPALART, P. R., ROGERS, M. M. & MOSER, R. D. 1991 Spectral methods for the Navier–Stokes equations with one infinite and two periodic directions. *J. Comput. Phys.* **96**, 297–324.

SQUIRES, K. D. & EATON, J. K. 1991 Preferential concentration of particles by turbulence. *Phys. Fluids* A **3**, 1169–1178.

STOKES , G. G. 1851 On the effect of the internal friction of fluids on pendulums. *Trans. Camb. Phil. Soc.* **9**, 8–106.

TANG, L., WEN, F., YANG, Y., CROWE, C. T., CHUNG, J. N. & TROUTT, T. R. 1992 Self organizing particle dispersion mechanism in a plane wake. *Phys. Fluids* A **4**, 2244–2251.

THEODORSEN, T. 1952 Mechanism of turbulence. In *Proc. 2nd Midwestern Conf. on Fluid Mech.* Ohio State University, Columbus, Ohio (cited in S. K. Robinson 1991).

WANG, L. P. & MAXEY, M. R. 1993 Settling velocity and concentration distribution of heavy particles in homogeneous isotropic turbulence. *J. Fluid Mech.* **256**, 27–68.

WRAY, A. A. & HUNT, J. C. R. 1989 Algorithms for classification of turbulent structures. In *Topological Fluid Mechanics* (ed. H. K. Moffatt & A. Tsinober), pp. 95–104. Cambridge University Press.